Failure properties of intraluminal thrombus in abdominal aortic aneurysm under static and pulsating mechanical loads

T. Christian Gasser, PhD,[a] Göray Görgülü, MSc,[a] Maggie Folkesson, MSc,[b] and **Jesper Swedenborg, MD, PhD,[b]** *Stockholm, Sweden*

Objectives: **It has been suggested that mechanical failure of intraluminal thrombus (ILT) could play a key role in the rupture of abdominal aortic aneurysms (AAAs), and in the present study, this hypothesis has been investigated. An in vitro experimental approach has been proposed, which provides layer-specific failure data of ILT tissue under static and pulsatile mechanical loads.**

Methods: **In total, 112 bone-shaped test specimens are prepared from luminal, medial, and abluminal layers of eight ILTs harvested during open elective AAA repair. Three different types of mechanical experiments, denoted as control test, ultimate strength test, and fatigue test were performed in Dulbecco's modified eagle's medium (DMEM) supplemented with fetal calf serum, L-ascorbic acid, and antibiotics at 37°C and pH 7.0. In detail, fatigue tests, which are experiments, where the ILT tissue is loaded in pulsatile manner, were carried out at three different load levels with a natural frequency of 1.0 Hz.**

Results: **ILT's ultimate strength (156.5 kPa, 92.0 kPa, and 47.7 kPa for luminal, medial, and abluminal layers, respectively) and referential stiffness (62.88 kPa, 47.52 kPa, and 41.52 kPa, for luminal, medial, and abluminal layers, respectively) continuously decrease from the inside to the outside. ILT tissue failed within less than 1 hour under pulsatile loading at a load level of 60% ultimate strength, while a load level of about 40% ultimate strength did not cause failure within 13.9 hours.**

Conclusions: **ILT tissue is vulnerable against fatigue failure and shows significant decreasing strength with respect to the number of load cycles. Hence, after a reasonable time of pulsating loading ILT's strength is far below its ultimate strength, and when compared with stress predictions from finite element (FE) studies, this indicates the likelihood of fatigue failure in vivo. Failure within the ILT could propagate towards the weakened vessel wall behind it and could initialize AAA failure thereafter. (J Vasc Surg 2008;48:179-88.)**

Clinical Relevance. **Rupture of an abdominal aortic aneurysm is the 10th leading cause of death in men above 60 years of age. Diameter of the aneurysm, the only accepted parameter to determine its rupture risk, is unreliable, and there is need for others. Aneurysm rupture has been related to growth of the intraluminal thrombus and failure of it might indicate a rupture risk. We demonstrate here that the strength of thrombus tissue decreases significantly under pulsating mechanical loads, a material characteristic to be known as fatigue. The derived data highlight the biomechanical role of the thrombus in abdominal aortic aneurysms, and therefore, improved risk prediction criteria could be drawn from that finding.**

The prevalence of abdominal aortic aneurysms (AAAs) ranges from 2.0%[1] to 8.8%[2] in the elderly population and AAA repair causes high socioeconomic costs.[3,4] AAA rupture has a mortality rate of 90%,[5] and death from ruptured AAAs is the 10th leading cause of death in men above the age of 65.[6]

From the Department of Solid Mechanics, Royal Institute of Technology (KTH)[a] and the Department of Vascular Surgery, Karolinska University Hospital and Institute.[b]

Competition of interest: none.

Reprint requests: T. Christian Gasser, PhD, Royal Institute of Technology (KTH), Department of Solid Mechanics, Osquars backe 1, SE-100 44 Stockholm, Sweden (e-mail: tg@hallf.kth.se).

0741-5214/$34.00

doi:10.1016/j.jvs.2008.01.036

An intraluminal thrombus (ILT) is found in nearly all AAAs with a diameter large enough to indicate risk of rupture.[7] The ILT is thought to play an important role in the pathology and natural history of AAA with multiple effects on the underlying vessel wall. The ILT causes localized hypoxia, possibly leading to increased neovascularization, inflammation, and regional weakening,[8] as well as changes of matrix-degrading protease expression[9] and structural and cellular composition[10] of the underlying AAA wall. ILT has a significant structural impact on the biomechanics of AAAs and influences both the magnitude and the distribution of AAA wall stress.[11-14]

Clinical studies indicate that the growth rate of the ILT may be of importance for the prediction of AAA rupture and expansion.[15-17] In a study examining computed to-

Table. Patient specific data of the investigated ILTs

Patient	*Gender*	*Age (Years)*	*Smoking*	*Max. AAA diameter (mm)*	*Max. ILT thickness (mm)*
1028	Male	80	Previous	50	[a]
1033	Female	70	Yes	50	27
1040	Male	73	Yes	57	23
1044	Male	70	No	54	28
1045	Female	68	Previous	59	23
1048	Male	65	Previous	70	24
1051	Male	82	Previous	60	22
1052	Female	71	Yes	66	28

ILT, Intraluminal thrombus; *AAA,* abdominal aortic aneurysm.
[a]Could not be measured from computed tomography without contrast.

mography (CT) findings of ruptured AAA, the maximal diameter of the thrombus, however, was not significantly different when comparison was made with unruptured AAA.[18] On the other hand, the strength of the wall under the thrombus and the risk of rupture have been reported to be negatively influenced by the thickness of the thrombus.[19]

It has been reported that that AAA rupture is initiated by blood entering the ILT identified as a "crescent sign" on CT examinations.[20,21] Detailed evaluation of signs of rupture from CT data emphasize that the majority of AAA failures occur in the wall underlying the ILT or in the immediate vicinity of it.[22,23] Hence, beside the failure properties of the wall,[19] those of the ILT may play a role to assess the risk of aneurysm rupture. Note that the ILT, although a weak tissue, can be several times thicker than the wall, thus, it might substantially contribute to the overall strength of the AAA.

In contradiction to experimental findings,[20,21] finite element (FE) calculations of AAAs indicate that the mechanical stress level in the ILT in vivo remains too low, when compared with its ultimate rupture strength, to cause failure therein.[14] These opposite findings leave the role of ILT in a rupture risk assessment of AAAs an open question, thus, necessitating further research to provide answers to this important scientific and clinical question. The FE method[31] divides a structure into a finite number of individual elements, and, in the present context, it has been used to investigate the mechanical loading of AAAs.

A thrombus is a complex structure, where aggregated platelets and other blood elements are trapped within a fibrin mesh traversed by a continuous network of interconnected canaliculi.[24] Mechanical testing has shown that ILT tissue can be regarded as an isotropic and linear material,[25,26] which withstands high deformations until failure.[13,25] Likewise, stiffness and strength decrease from inside to the outside whereas the time dependent (viscoelastic) properties remain constant across the thickness.[27] ILT's ultimate strength, eg, as identified by quasi-static rupture tests,[13,25] where the mechanical load on a test specimen is slowly increased until the tissue specimen fails, might considerably overestimate the failure strength of the ILT in vivo. A pulsatile blood pressure causes cyclic mechanical loading of ILT tissue, which most likely activates fatigue-like failure mechanisms at stress levels much below the ILT's ultimate strength. To explore that hypothesis, ie, whether or not ILT is vulnerable to fatigue failure, the present study introduces an in vitro experimental approach and presents novel experimental data particularly useful to interpret stress predictions from FE models of AAA. To this end, pulsating tensile load is applied to bone-shaped test specimens aligned with the ILT's circumferential direction, hence, along which the dominating mechanical (in vivo) loading is expected.

METHODS

Specimen preparation. ILT samples (n = 8) were harvested from AAAs during surgical elective repair, put in Dulbecco's modified eagle's medium (DMEM), supplemented with 20% fetal calf serum (FCS), 50 μg/mL L-ascorbic acid, 50 μg/mL streptomycin, 50 IU/mL penicillin, and kept on ice (for a maximum of 3 hours) and then at −35°C (for 1 to 9 weeks). The collection and use of ILT material from human subjects was approved by the local ethics committee and detailed specifications of the study subjects are given in the Table.

Prior to the preparation of test specimens, ILT samples were thawed at +4°C for 24 hours. After stabilization at room temperature (20°C) for about 30 minutes, each ILT bulk tissue was first divided into the layers illustrated in Fig 1 to gather tissue sheets from different structural layers. The thickness of the separated sheets ranged from 1.0 to 2.0 mm and according to their location within the bulk ILT tissue, they are labeled as luminal, medial and abluminal throughout the following procedure. From each sheet, four uniaxial bone-shaped specimens, each oriented in circumferential direction, were punched out with an especially developed pattern blade (see Fig 1, *e*). If case the sheet was large enough, a fifth specimen, ie, a control specimen, was prepared as a reference for the testing protocol.

To improve the fixation of the specimen in the testing machine, sand paper pieces were attached to their ends using super-adhesive glue (LOCTITE). Careful application of the optimal glue amount was proven to be crucial in order to avoid failure at the ends instead of the middle of the specimen. The preparation of luminal, medial, and abluminal test specimens out of the bulk ILT tissue is

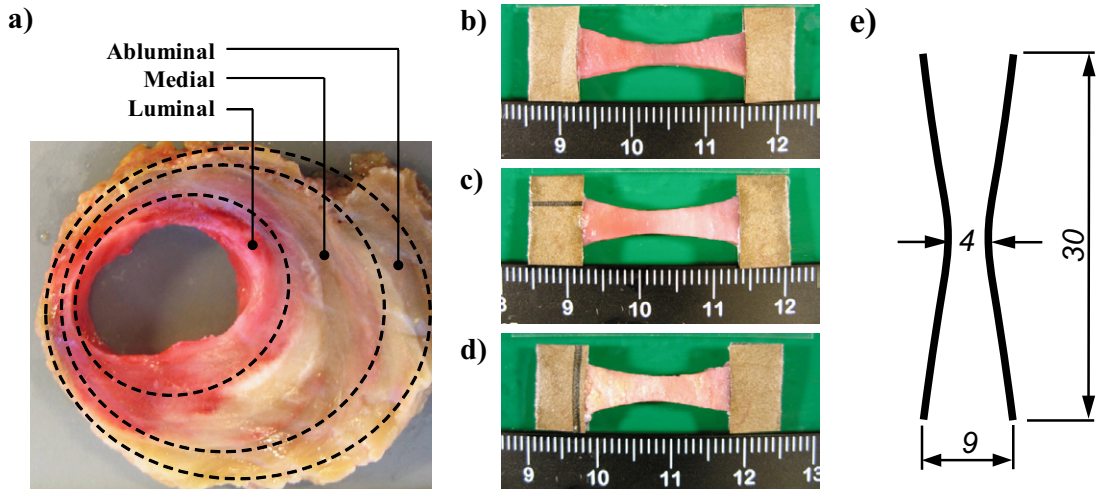

Fig 1. Preparation of uniaxial test specimens. **a,** Cross-section of the bulk intraluminal thrombus tissue harvested from elective abdominal aortic aneurysm repair, where luminal, medial, and abluminal layers are indicated. Sample uniaxial test specimens prepared from (**b**) luminal, (**c**) medial, and (**d**) abluminal layers, respectively. **e**, Dimensions of the pattern blade.

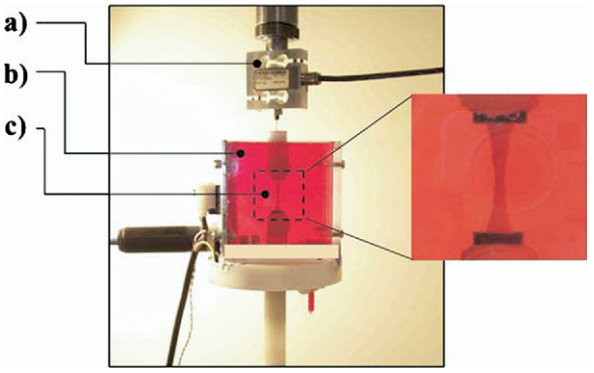

Fig 2. Part of the testing equipment illustrating (**a**) the load-cell, (**b**) the tissue testing chamber filled with Dulbecco's modified eagle's medium, and (**c**) the test specimen fixed between two PVC grips.

illustrated in Fig 1, and it is emphasized that the specimens were kept hydrated during the whole preparation process.

Specimens were uniquely identified and stored in DMEM (with supplements) at +4°C until the mechanical testing and a total number of 112 test specimens were prepared.

Testing equipment. ILT testing was performed on a uniaxial testing machine (MTS 305.03/30 kN, Eden Prairie, Minn) equipped with a control unit (INSTRON 8500 Plus, Norwood, Mass) including a hydraulic actuation tower and a digital control panel (Figs 2 and 3). Entire set of experiments was conducted in displacement control mode, where the load on specimens was measured by a 10N-load cell (VETEK TCA/1.0 kg, Vaddo, Sweden) and the data were recorded by an ordinary personal computer. During testing, ILT specimens were kept in DMEM (with supplements) at 37°C (±0.5) and pH of 7.0 (±0.6) to ensure physiological conditions close to the in vivo situation. The versatile liquid composition was particularly essential to prevent the ILT tissue from degradation during the lengthy fatigue cycles, which was observed during preliminary testing in Ringer solution at 37°C (±0.5). DMEM (with supplements) was kept in a 0.5 l test chamber of polymethyl methacrylate (PMMA) with a top lid to reduce loss by evaporation.

The constant testing temperature of 37°C (±0.5) was ensured by a temperature sensor (OMRON Pt-100, Kyoto, Japan), an especially developed heating plate and a digital temperature controller (OMRON E5GN). In addition, pH of the DMEM (with supplements) was measured by a pH electrode (COLE-PARMER CZ-27001-70, Vernon Hills, Ill) and displayed. DMEM (with supplements) was replaced if pH exceeded its target range of 7.0 (±0.6).

The ILT specimen was gripped with especially developed grips entirely made of polyvinyl chloride (PVC), where the upper grip is attached to the load cell using a tension string made of the synthetic polyester fiber terylene. This design reduces bending forces possibly entering the testing specimen, and hence, assures a uniform distribution of the tensile stress throughout its cross-section.

Testing protocols. Uniaxial mechanical tests conducted on ILT specimens were of three different types: control test, ultimate strength test, and fatigue test. From the 112 prepared specimens 6, 24, and 72 were dedicated to the control tests, ultimate strength tests, and fatigue tests, respectively.

The control test aims to investigate (control) ILT tissues' (pseudo-)elastic properties in the testing environment over a time period of 2 days. The underlying load level was defined as $0.3P_{ult}$ (ie, small enough to remain below the elastic limit of the tissue), where P_{ult} denotes the ultimate

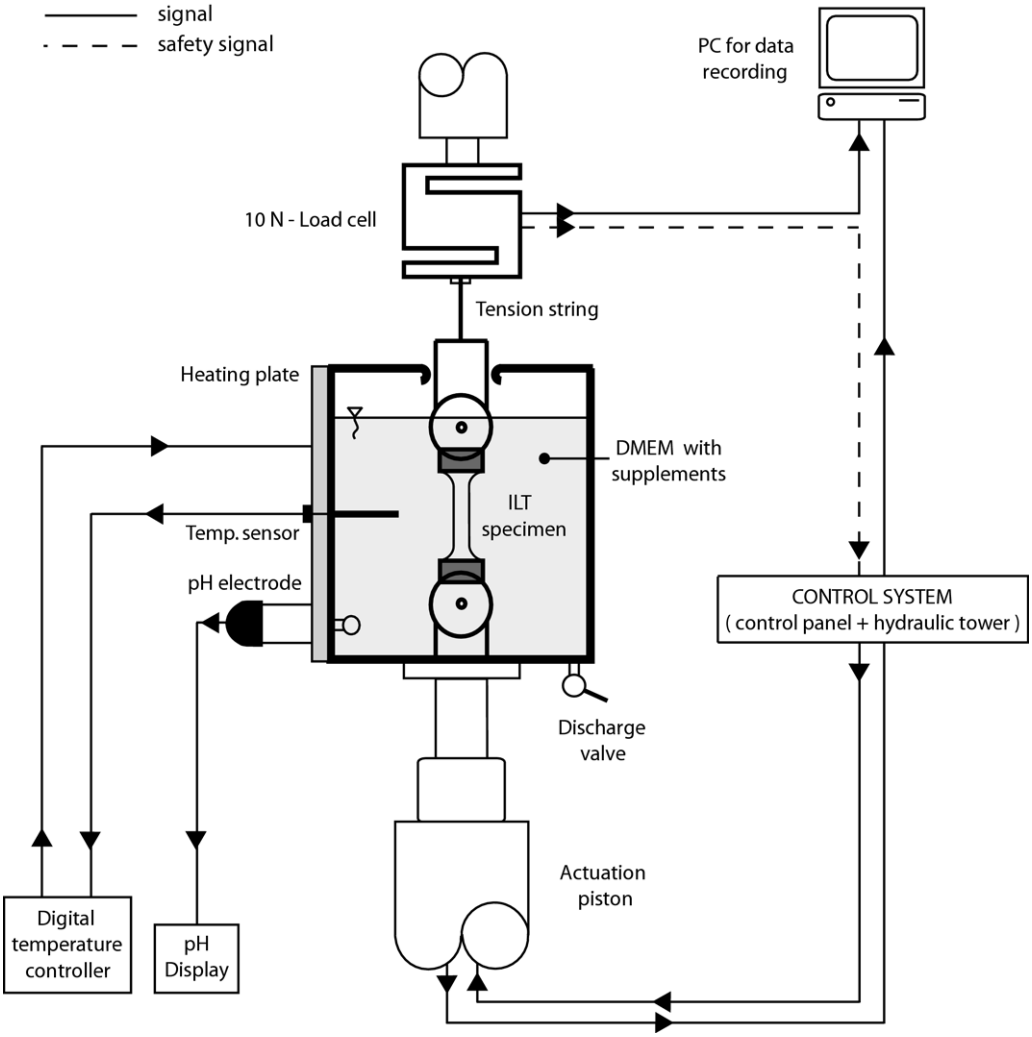

Fig 3. Experimental set-up used to test intraluminal thrombus (ILT) tissue under static and pulsating mechanical loads. Displacements are applied by the actuation piston and the load is measured by the 10N-Load cell. The ILT specimen is kept in Dulbecco's modified eagle's medium, whose temperature is controlled and pH is displayed.

strength of the ILT sheet under investigation. The control specimen was tested every 12 hours; it was first preconditioned through six cycles and test data were recorded from the following three repetitive tension cycles. The elongation rate of 0.2 mm/s was applied, and hence, the test can be regarded as quasi-static. Between testing, the specimen stayed unloaded in the DMEM (with supplements) at 37°C (± 0.5) and pH of 7.0 (± 0.6).

For the ultimate strength test the specimen was elongated at 0.2 mm/s until failure, where no preconditioning was considered. Load and displacement were recorded and the ultimate load F_{ult} defined the tissue's ultimate strength $P_{ult} = F_{ult}/A$ by means of the first Piola-Kirchhoff stress,[28] where A is the referential cross section of the specimen at which failure appears, ie, at its most slender portion. Again, the low elongation rate ensures quasi-static test conditions. Fatigue tests, as the main focus of this study, were performed at the natural frequency of 1.0 Hz, where the shape and (initial) amplitude of the fluctuating load were assumed to be sinusoidal in time and 0.2 times the mean (initial) load level P_m, respectively. Throughout this study, three different (initial) mean load levels were considered, $0.5P_{ult}$, $0.7P_{ult}$, and $0.9P_{ult}$, where P_{ult} denotes the ultimate strength of the ILT sheet being investigated. From Solid Mechanics, it is well understood that stress peaks appear at sharp edges, and hence, these stress levels (although thought to be high) might appear even under physiologic conditions. Note that the test was conducted in displacement control, and hence, the displacement was kept constant while the amplitude and mean load decreased over time. Prior to cyclic loading the specimen was constantly elongated at 0.2 mm/s until the mean load P_m was reached and data was evaluated up to 50×10^3 cycles thereafter. The loading protocol for fatigue testing is summarized in Fig 4.

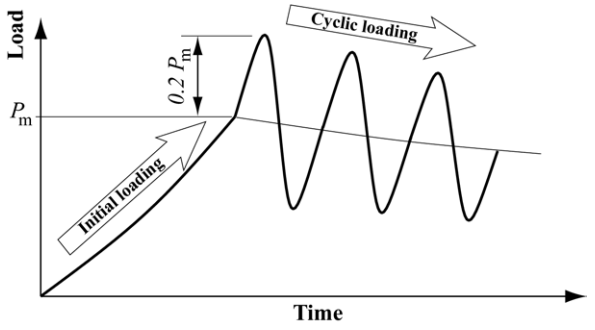

Fig 4. Illustration of the loading protocol for the fatigue testing. Displacement controlled initial loading at 0.2 mm/s up to the mean load level P_m followed by displacement controlled cyclic (*sinusoidal*) loading at 1.0 Hz and $0.2P_m$ initial amplitude.

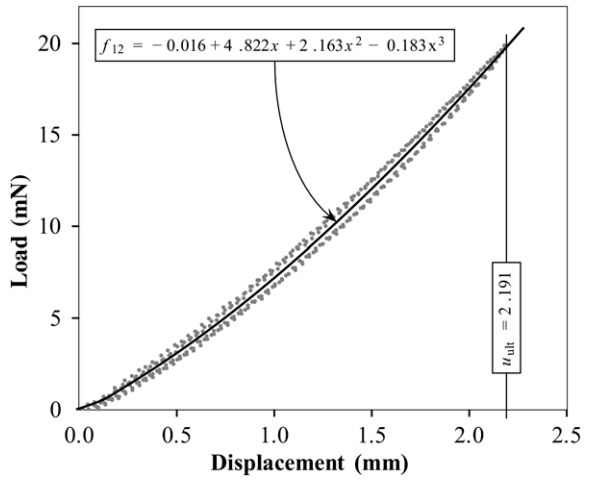

Fig 5. Analytical representation of the control test data. Gray dots show experimental data from three repetitive tension cycles of a intraluminal thrombus specimen, which has been kept in Dulbecco's modified eagle's medium at 37°C (±0.5) and pH of 7.0 (±0.6) for 12 hours. A third order polynomial f_{12} is used to represent the mean loading-unloading behavior, and hence, to quantify the specimen's stiffness at that time.

RESULTS

Control test. Results from the control test emphasize that the ILT shows mechanical properties typical for soft biological tissues like preconditioning phenomena and pseudo-elasticity.[29] Unusual for soft biological tissues, an almost linear relation of the load with respect to specimen elongation was observed indicating that the ILT exhibits a linear stress-strain behavior[26] (see Fig 5). In order to quantify the changes of the ILT's elastic properties over time in DMEM (with supplements) at 37°C (±0.5) and pH of 7.0 (±0.6), the recorded data of the particular repetitive tension cycles were fitted to third order polynomials f_i,i = 0, 12, 24, 36, 48 in a least-square sense.[30] The analytical descriptions f_i represent the average of the loading and unloading branches at 0, 12, 24, 36, and 48 hours, ie, the

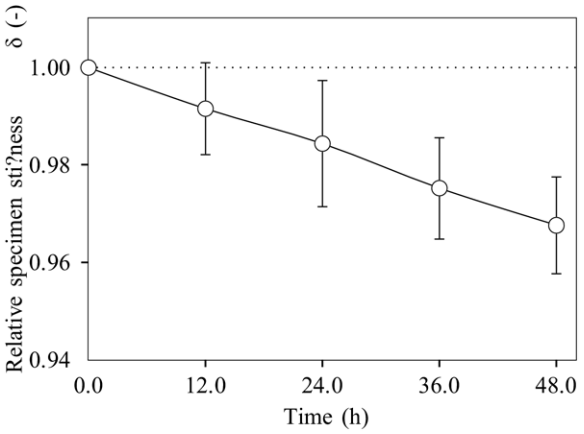

Fig 6. Evolution of the relative elastic specimen stiffness δ_i over time in Dulbecco's modified eagle's medium at 37°C (±0.5) and pH of 7.0 (±0.6). Error bars denote standard deviation associated with patient heterogeneity. The intraluminal thrombus specimens weaken over time, however, their elastic stiffness changes less than 3.5% within 48 hours.

average of the three repetitive tension cycles recorded at those times. An example is illustrated in Fig 5, where the recorded experimental data (shown by gray dots) from a control specimen, which has been kept in DMEM (with supplements) for 12 hours is represented by the analytical description f_{12} (shown by the solid line).

Based on the analytical descriptions f_i, the change of ILT's elastic properties over time is quantified by the relative specimen stiffness $\delta_i = \bar{K}_i/\bar{K}_0$, $i = 0, 12, 24, 36, 48$. Here

$$\overline{K_i} = \frac{1}{u_{ult}} \int_0^{u_{ult}} \left(\frac{df_i}{du} \right) du = \frac{1}{u_{ult}} \left(f_i\left(u_{ult}\right) - f_i\left(0\right) \right)$$

has been introduced, where u_{ult} denotes the displacement at the ultimate load F_{ult} (see Fig 5). $\overline{K_i}$ denotes the average specimen stiffness at time i, and δ_i relates it to its stiffness $\overline{K_0}$ at the beginning of the control test.

The evolution of the relative specimen stiffness δ_i over time is illustrated in Fig 6, where an almost linear softening tendency over time is exhibited. However, δ_i remains larger than 0.965, which means that the elastic stiffness of the ILT samples change less than 3.5% within 48 hours. Note that the duration of the fatigue tests performed within this study was at maximum 13.9 hours, and hence, the testing environment had a negligible effect on the elastic properties of ILT tissue.

Ultimate strength test. Apart from base data for the subsequent tests, the ultimate strength tests provided detailed data regarding the variation of ILT tissue stiffness and ultimate strength across its radial direction, ie, from the inner tissue towards the outer tissue. Again, the raw data revealed an approximately linear relation of the recorded force with respect to specimen elongation. Note that the nonhomogeneous strain field caused by the bone-shaped

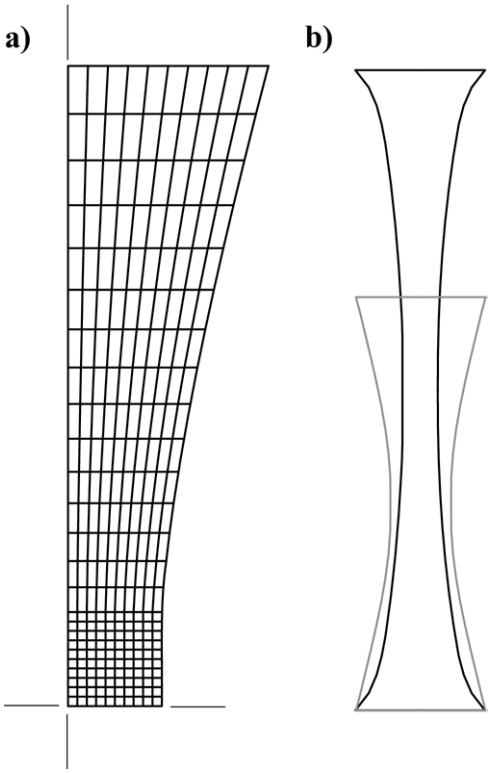

Fig 7. Plane stress FE model of a particular intraluminal thrombus specimen to extract the material parameters from recorded experimental data. **a,** Applied finite element discretization of a quarter of the specimen. **b,** Gray and black outlines illustrate the referential and the deformed configurations of the modeled test specimen, respectively.

specimens leads to a mix of configuration and material effects, such that the test results do not allow an immediate quantification of the material's constitution.

In order to facilitate ILTs constitution, ie, to distinguish the mechanical properties of ILT material from the configurational effects of the bone-shaped test specimen, an elastic two-dimensional (plane stress) FE computation was performed from each ultimate strength test. In particular, a quarter of the specimen, (see Fig 7, *a*) was discretized (split into individual elements) and associated loading conditions were applied.

The incompressible mechanical properties of ILT tissue were modeled by the one parameter Ogden-like strain energy function.[28]

$$\psi = c\sum_{i=1}^{3}\left(\lambda_i^4 - 1\right) \qquad (1)$$

where the material parameter c needs to be determined from experimental data. In eq (1), λ_i, $i = 1, \ldots, 3$ denotes the $i-$th principal stretch, which describes tissue elongation along the $i-$th principal direction. The principal directions span an orthogonal coordinate system, within which the state of deformation is free of shear, and each deformation can be described by the principal stretches and associated principal directions.[28] Eq (1) entirely describes ILT's constitution and standard arguments[28] define the principal Cauchy (or true) stress $\sigma_i = \lambda_i \partial\psi/\partial\lambda_i - p$, $i = 1, 2, 3$ depended on the principal stretches λ_i and the hydrostatic pressure p. The Cauchy stress is the mechanical load acting at the deformed area element of the tissue,[28,32] and $\partial\psi/\partial\lambda_i$ denotes the partial derivative of the strain energy function with respect to the i-th principal stretch.

The proposed constitutive model (1) predicts an approximately linear load-displacement response within the considered range of tissue deformations, and hence, is able to capture the experimental findings of ILT tissue satisfying. The material parameter c was identified by comparing the FE prediction (which itself depends on c) with the experimentally recorded load-displacement data of a particular ultimate strength test. To this end, c was iteratively updated until agreement in a least square sense[30] was achieved. An FE prediction of a particular ultimate strength test, ie, its deformation due to tensile loading, is illustrated in Fig 7, *b*, where the referential (stress-free) and the deformed (right before failure) configurations are shown by the gray and black outlines, respectively. In Fig 8, the distribution of the material parameter c along the radial direction of the ILT is plotted, where a considerable decrease between luminal and medial layers passes into a slight difference between medial and abluminal layers. In summary, the material parameter c of the luminal, medial and abluminal ILT can be quantified to 2.62 kPa (SD 0.80), 1.98 kPa (SD 0.62), and 1.73 kPa (SD 0.64), respectively, ie, ILT stiffness decreases about linearly by 44% from the luminal to the abluminal tissue.

Note that the standard deviation (SD) is associated with patient heterogeneity, and it is emphasized that the referential shear modulus $\mu = 8c$ and the stiffness $E = 24c$ of the material are uniquely defined by the introduced model (1). For sake of completeness μ and E are included in Fig 8.

Apart from defining the material parameter c, the applied mixed numerical and experimental analysis is able to evaluate the Cauchy stress at (right before) ILT failure, ie, to define ILT's ultimate strength in a spatial setting. Note that the computation of the Cauchy stress requires detailed knowledge of the tissue's state of deformation (Cauchy stress refers to the deformed area element), and hence, cannot directly be evaluated from the experimental data provided by the set-up described in the Methods section. The estimated ultimate strength of ILT tissue in terms of Cauchy stress is illustrated in Fig 9, where a considerable decrease from the inside to the outside is observed. In summary, the ultimate strength of the luminal, medial, and abluminal ILT have been determined as 156.5 kPa (SD 57.9), 92.0 kPa (SD 37.5), and 47.7 kPa (SD 22.9), respectively. Hence, ILT ultimate strength decreases about linearly by 70% from the luminal to the abluminal tissue.

Fatigue test. The typical load-cycle behavior of the fatigue test is illustrated in Fig10, where the recorded data of particular $0.9P_{ult}$, $0.7P_{ult}$, and $0.5P_{ult}$ load cases are

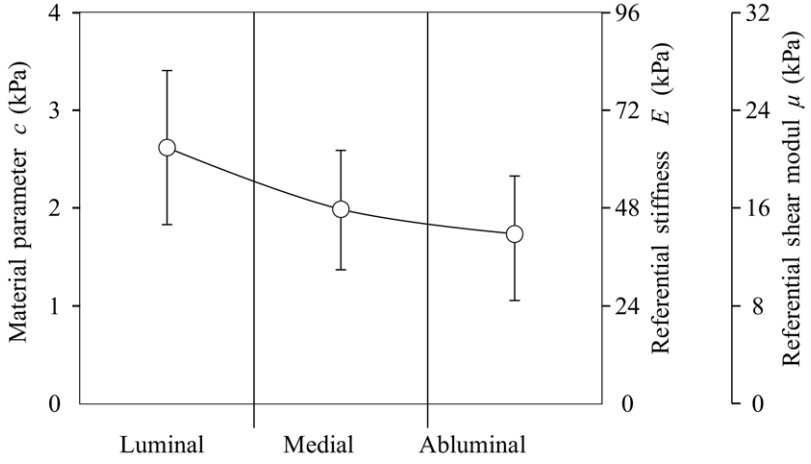

Fig 8. Variation of intraluminal thrombus (ILT) stiffness across the radial direction represented by data from luminal, medial and abluminal specimens. Error bars denote standard deviation associated with patient heterogeneity. ILT stiffness decreases about linearly by 44% from the luminal to the abluminal tissue.

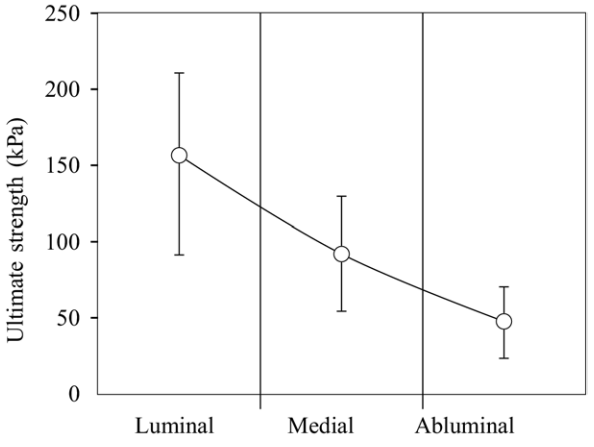

Fig 9. Variation of intraluminal thrombus (ILT) ultimate strength in terms of Cauchy (or true) stresses across the radial direction represented by data from luminal, medial and abluminal specimens. Error bars denote standard deviation associated with patient heterogeneity. ILT ultimate strength decreases about linearly by 70% from the luminal to the abluminal tissue.

plotted with respect to the number of load cycles. The $0.9P_{ult}$ and $0.7P_{ult}$ load cases resulted in failures (indicated by the circles) after 89 and 466 cycles, whereas the $0.5P_{ult}$ load cases did not fail within 50×10^3 cycles. At the beginning of the tests, all three cases showed about the same decrease in load. For the $0.5P_{ult}$ load case, the slow decay in the beginning turns into a much faster one as the cycles continue, remaining with a constant slope until the test is terminated. Similar initial decays are exhibited by the $0.7P_{ult}$ and $0.9P_{ult}$ load cases; however, the load declines are progressive prior to failure.

Throughout the fatigue tests, all specimens (initially) loaded at $0.9P_{ult}$, 33.3% of the specimens (initially) loaded at $0.7P_{ult}$, and none of the specimens (initially) loaded at $0.5P_{ult}$ failed under the pulsatile loading. Since no significant difference amongst luminal, medial, and abluminal layers could be observed, the data have been pooled and summarized in the Wöhler-curve (also known as S-N curve) of Fig 11. To this end, the normalized First Piola-Kirchhoff stress

$$\bar{P} = \frac{\sum_{i=1}^{n_{fail}} P_i}{n_{fail} P_{ult}}$$

which acts in average over the duration of the experiment, is plotted versus the number of load cycles n_{fail} prior to failure. Here, P_i denotes the mean First Piola-Kirchhoff stress acting in the most slender cross section of the specimen over the $i-$th load cycle. The First Piola-Kirchhoff (or engineering) stress relates the mechanical load to the undeformed area,[28,32] thus, it can be directly derived from the experimental data and the test specimen's unloaded geometry.

Those fatigue tests, where the specimen failed during the experiment, are represented by data points in Fig 11 and regression analysis[30] was applied to define a linearly decreasing curve with slope $\Delta\bar{P}/\Delta\log(n_{fail}) = -0.545$. This curve (shown as dashed line in Fig 11) represents the vulnerability of ILT tissue against fatigue failure emphasizing its decreasing strength with respect to the number of load cycles. For this representation of the data, the results from the ultimate strength tests collapse in (1.0, 1.0) and the curve was enforced to pass this point. Likewise, circles and squares are used to indicate the data points from the $0.9P_{ult}$ and $0.7P_{ult}$ load cases, respectively.

Assuming the deformation of the test specimen does not change from cycle to cycle, Fig 11 also represents the normalized Cauchy stress with respect to the number of load cycles. Since the overall deformation (defined by the clamp displacement) of the displacement controlled fatigue test was the same from cycle to cycle, this assumption holds

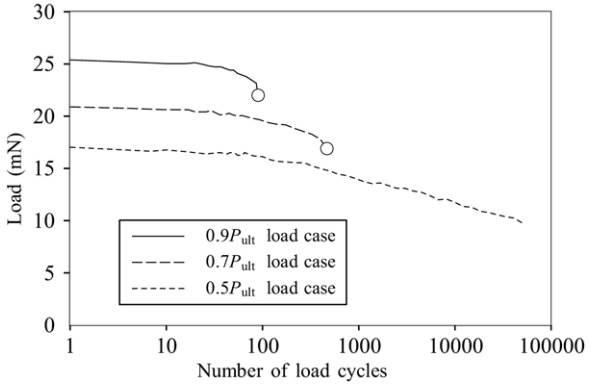

Fig 10. Example data recorded during the fatigue tests of a particular luminal sheet of intraluminal thrombus (ILT). Load cycle behaviors of three specimens are plotted with respect to the logarithmic number of load cycles. The specimens were initially loaded at 0.9, 0.7, and 0.5 times the ultimate strength (P_{ult}) of the ILT sheet they had been prepared from.

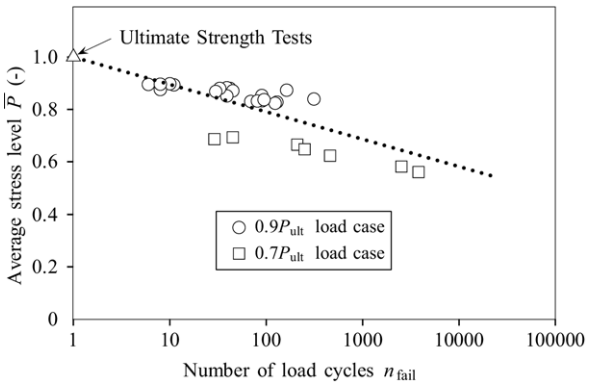

Fig 11. Wöhler-curve representing the vulnerability of intraluminal thrombus (ILT) tissue against fatigue failure, ie, decreasing strength with respect to the number of load cycles. Fatigue tests, where the ILT specimen failed during the experiment, are represented by (*circular and rectangular*) data points and the dashed line is defined by regression analysis.

if the redistribution of the strain field due to inelastic deformations is negligible.

For completeness, it is worth noting, that the specimens (initially) loaded at $0.7P_{ult}$ and did not fail within 50×10^3 load cycles, showed a normalized First Piola-Kirchhoff stress $\bar{P} = 0.392$ SD (0.064) in average over the duration of the experiment.

Finally, a remarkable stress relaxation, ie, decreasing load over time, has been observed during the experiments (see Fig 10). In order to investigate this phenomena in more detail, we focused on the $0.5P_{ult}$ load case only. To this end, we assumed that the mean First Piola-Kirchhoff stress P (in the middle of the specimen) can be represented by $P(\lambda, n) = G(n)P_0(\lambda)$, where λ and n denote the stretch (in the middle of the specimen) and the number of load cycles, respectively. Here, P_0 is the mean First Piola-Kirchhoff stress at the beginning of the fatigue test, and $G(n)$ is a dimensionless stress-relaxation function to be determined from experimental data. Note that this multiplicative decomposition of the stress states an established concept to describe soft tissue viscoelasticity.[33]

The observed stress relaxation behavior (see Fig 10) motivates the introduction of a bi-linear function for $G(n)$ with respect to the logarithmic number of load cycles, and hence, allow the quantification of three material parameters, ie, its initial k_i and final k_f slopes and the number of load cycles n_{tran} at the transition point. In addition, the observed stress relaxation did not change amongst luminal, medial, and abluminal specimens, and hence, the data were pooled. Finally, regression analysis quantified the material parameters $k_i = -7.94\times10^{-3}$ (SD 4.22×10^{-3}), $k_f = -7.32\times10^{-2}$ (SD 1.89×10^{-2}) and $\log n_{tran} = 6.09$ (SD 0.99), which define the bi-linear stress-relaxation function $G(n)$.

DISCUSSION

The present study highlights that ILT tissue is vulnerable against fatigue and fails at load levels far below its ultimate strength under pulsatile loading. More specifically, we observed failure within less than 1 hour at a mean load level of 60% ultimate strength, whereas a load level of about 40% did not cause failure within 13.9 hours.

While failure of traditional engineering materials has been extensively investigated over the past decades,[34] little is yet known about failure in vascular tissues.[35-37] In particular, the evolution of fatigue damage in vascular tissues is a completely unexplored field in biomechanics, and to our knowledge, the present study is the first attempt to investigate ILT's fatigue properties. The experiments in the present study were limited to 13.9 hours, and it is likely that, ILT strength would have further decreased with increasing number of load cycles. As a matter of fact, living tissue has the capability to compensate for the evolution of damage by healing mechanisms, as it is known from bone tissue, where basic multicellular units (BMU) replace the old with new material.[38] Hypothetically, the ILT tissue could have such functionality, however, not towards the abluminal layer, where one faces a more or less inert material.

A comparison of ILT's failure strength under pulsatile loading with stress fields obtained from FE studies reported in the literature (for instance; peak stress of 30.0 to 110.0 kPa in the ILT[14]) indicates that in vivo fatigue failure of ILT tissue becomes a possible scenario. Once a macroscopic failure in the ILT has been formed, it could propagate towards the AAA wall, which itself could rupture due to the associated development of a stress concentration. Note that the aneurysm wall is remarkably weaker[8] and thinner[10] behind (thick) ILTs when compared with the ILT-free wall. This failure mechanism could explain that the majority of AAA ruptures are found behind the ILT,[22,23] and consequently, it suggests that the ILT is a major player in the pathogenesis of AAA rupture. Although ILT strength is

only a small fraction of the AAA wall strength, it is several time thicker, which underlines its substantial contribution to the overall strength of the AAA. The assumption that the ILT fails prior to the wall (and not vice versa) is motivated by the fact that the highest and lowest circumferential stresses in pressurized thick-walled tubes are at the inside and outside, respectively.

Most ILTs are firm and white except for the luminal layer. Occasionally, soft and friable red ILT are encountered. Such ILT were not found during the collection of ILT in the present study. Furthermore, it would have been impossible to test these loose thrombi with the present technique.

The present study has shown that the testing solution, in which the ILT tissue was kept during the lengthy experiments, plays a crucial role to achieve reliable results. All mechanical tests were done in DMEM, supplemented with FCS, L-ascorbic acid and antibiotics at 37°C (±0.5) and pH of 7.0 (±0.6). Furthermore, solution medium's impact on the elastic mechanical properties of ILT has been carefully observed by control tests. It was found that, over 48 hours, which is about four times the duration of the longest fatigue testing, the elastic properties of ILT did not change significantly. Yet, no conclusion can be drawn regarding the evolution of its inelastic properties. Similarly, the time the ILT was kept frozen had a negligible impact on the on the results compared to patient heterogeneity.

A sinusoidal displacement controlled loading, where the initial amplitude is linked to the initial mean load, was prescribed for the fatigue tests in the present study. The cyclic in vivo loading of ILT tissue however is more complicated, eg, the amplitude and shape of the fluctuation (both load and displacement) will vary over time, particularly at locations where macro-failure develops. It is known from traditional engineering materials that the amplitude and shape of fluctuating load affects the life time predictions, which needs to be considered, when interpreting results from the present study.

The displacement controlled fatigue test was accompanied by a significant reduction of the loading over time (stress relaxation), such that the stress level at high numbers of load cycles became too small to initialize failure thereat. Consequently, a load controlled testing protocol, instead of displacement controlled one applied herein, seems to be more suitable to investigate the fatigue failure of pronounced viscoelastic materials like ILT tissue at higher load cycles.

Likewise, smaller load steps between the different fatigue tests would refine the provided data. The performed ultimate strength tests have revealed the variation in mechanical properties of ILT tissue along its radial direction in accordance with its structural changes,[24] and as reported earlier.[25] Previous studies reported a circumferential strength of the luminal ILT by the First Piola-Kirchhoff stress of 85.0 kPa (SD 47.0),[13] and for luminal and medial ILT by the Cauchy stresses of 540.0 kPa (SD 70.0) and 220.0 kPa (SD 50.0), respectively.[25] While the first value is in the range of the present findings (its transformation to the spatial setting gives a Cauchy stress of 128.1 kPa), the other two values are much larger than the findings herein, ie, 156.5 kPa (SD 57.9) and 92.0 kPa (SD 37.5) for luminal and medial layers.

A detailed discussion of the quantified ILT stiffness with respect to the existing literature lacks, since different definitions have been used. However, to some extent, the present findings can be compared with the circumferential ILT stiffness of 131.0 kPa (SD 64.0)[13] and 201.0 kPa (SD 16.0)[26] for the luminal ILT, but they are much lower than 540.0 kPa (SD 70.0) and 270.0 kPa (SD 40.0) for luminal and medial layers,[25] respectively. Finally, it is worth noting that, although the present study significantly differs from shear experiments, the reported elastic shear modulus of 1.3 kPa[27] is much lower than the one that can be derived from the present work (20.96 kPa [SD 6.4], 15.84 kPa [SD 4.96], and 13.84 kPa [SD 5.12], for luminal, medial, and abluminal layers, respectively).

In the present study, 1D loading in ILT's circumferential direction was considered to investigate its failure properties. However, in-vivo, a multi-axial loading condition exists, where tensile loading in circumferential and axial directions as well as a radial compression appear. Multiaxial loading influences fatigue phenomena and reduces the failure strength, shown to be valid for at least traditional engineering materials, and hence, it is likely the circumferential strength of ILT will decrease when additional axial tensile stress is superimposed.

Displacement controlled fatigue tests have shown considerable stress relaxation. Even though the underlying mechanisms such as viscoelasticity, poro-elasticity, and fatigue softening might be involved in the relaxation event, the individual role of each factor was beyond the scope of this study. In addition, experimental data have suggested that stress relaxation of ILT do not vary in radial direction, which is similar to its time dependent (viscoelastic) properties.[27] We believe that stress relaxation and the associated softening should certainly be considered in numerical models of AAAs; a softer ILT would redistribute the stresses from the ILT to the aneurysm wall, which could significantly change the mechanical loading situation of AAAs.

The authors gratefully acknowledge the technical contribution by Hans Öberg in the design and building up the experimental device, the assistance of Joy Roy and Anton Razuvaev in collecting ILT, and Gerhard Sommer for the helpful hints to prepare the test specimens. This work has been supported by the Young Faculty Grant No. 2006-7568 from the Swedish Research Council, VINNOVA, and the Swedish Foundation for Strategic Research, which are gratefully acknowledged.

AUTHOR CONTRIBUTIONS

Conception and design: GG, JS, MF, TG
Analysis and interpretation: GG, JS, TG
Data collection: GG, JS, MF
Writing the article: GG, JS, MF, TG
Critical revision of the article: JS, TG

Final approval of the article: GG, MF, JS, TG
Statistical analysis: GG, TG
Obtained funding: JS, TG
Overall responsibility: TG

REFERENCES

1. Bengtsson H, Sonesson B, Bergqvist D. Incidence and prevalence of abdominal aortic aneurysms, estimated by necropsy studies and population screening by ultrasound. Ann NY Acad Sc 1996;800:1-24.
2. Newman AB, Arnold AM, Burke GL, O'Leary DH, Manolio TA. Cardiovascular disease and mortality in older adults with small abdominal aortic aneurysms detected by ultrasonography: the cardiovascular health study 2001;134:182-90.
3. Bosch JL, Lester JS, McMahon PM, Beinfeld MT, Halpern EF, Kaufman JA, et al. Hospital costs for elective endovascular and surgical repairs of infrarenal abdominal aortic aneurysms. Radiology 2001;220: 492-7.
4. Jonk YC, Kane RL, Lederle FA, MacDonald R, Cutting AH, Wilt TJ. Cost-effectiveness of abdominal aortic aneurysm repair: a systematic review. Int J Technol Assess Health Care 2007;23:205-15.
5. Upchurch Jr GR, Schaub TA. Abdominal aortic aneurysm. Am Fam Phys 2006;73:1198-1204.
6. Vardulaki KA, Prevost TC, Walker NM, Day NE, Wilmink AB, Quick CR, et al. Growth rates and risk of rupture of abdominal aortic aneurysms. Br J Surg 1998;85:1674-80.
7. Hans SS, Jareunpoon O, Balasubramaniam M, Zelenock GB. Size and location of thrombus in intact and ruptured abdominal aortic aneurysms. J Vasc Surg 2005;41:584-8.
8. Vorp DA, Lee PC, Wang DH, Makaroun MS, Nemoto EM, Ogawa S, et al. Association of intraluminal thrombus in abdominal aortic aneurysm with local hypoxia and wall weakening. J Vasc Surg 2001;34: 291-9.
9. Kazi M, Zhu C, Roy J, Paulsson-Berne G, Hamsten A, Swedenborg J, et al. Difference in matrix-degrading protease expression and activity between thrombus-free and thrombus-covered wall of abdominal aortic aneurysm. Arterioscler Thromb Vasc Biol 2005;25:1341-6.
10. Kazi M, Thyberg J, Religa P, Roy J, Eriksson P, Hedin U, et al. Influence of intraluminal thrombus on structural and cellular composition of abdominal aortic aneurysm wall. J Vasc Surg 2003;38:1283-92.
11. Inzoli F, Boschetti F, Zappa M, Longo T, Fumero R. Biomechanical factors in abdominal aortic aneurysm rupture. Eur J Vasc Surg 1993;7: 667-74.
12. Mower WR, Quiãnones WJ, Gambhir SS. Effect of intraluminal thrombus on abdominal aortic aneurysm wall stress. J Vasc Surg 1997;33: 602-87.
13. di Martino ES, Mantero S, Inzoli F, Melissano G, Astore D, Chiesa R, et al. Biomechanics of abdominal aortic aneurysm in the presence of endoluminal thrombus: experimental characterization and structural static computational analysis. Eur J Vasc Endovasc Surg 1998;15: 290-9.
14. Wang DH, Makaroun MS, Webster MW, Vorp DA. Effect of intraluminal thrombus on wall stress in patient-specific models of abdominal aortic aneurysm. J Vasc Surg 2002;36:598-604.
15. Stenbaek J, Kalin B, Swedenborg J. Growth of thrombus may be a better predictor of rupture than diameter in patients with abdominal aortic aneurysms. Eur J Vasc Endovasc Surg 2000;20:466-99.
16. Satta J, Laara E, Juvonen T. Intraluminal thrombus predicts rupture of an abdominal aortic aneurysm. J Vasc Surg 1996;23:737-73.
17. Wolf YG, Thomas WS, Brennan FJ, Goff WG, Sise MJ, Bernstein EF. Computed tomography scanning findings associated with rapid expansion of abdominal aortic aneurysms. J Vasc Surg 1994;20:529-35.
18. Fillinger MF, Racusin J, Baker RK, Cronenwett JL, Teutelink A, Schermerhorn ML, et al. Anatomic characteristics of ruptured abdominal aortic aneurysm on conventional CT scans: implications for rupture risk. J Vasc Surg 2004;39:1243-52.
19. Vande Geest JP, Wang DH, Wisniewski SR, Makaroun MS, Vorp DA. Towards a noninvasive method for determination of patient-specific wall strength distribution in abdominal aortic aneurysms. Ann Biomed Eng 2006;34:1098-1106.
20. Arita T, Matsunaga N, Takano K, Nagaoka S, Nakamura H, Katayama S, et al. Abdominal aortic aneurysm: rupture associated with the high-attenuating crescent sign. Radiology 1997;2004:765-8.
21. Mehard WB, Heiken JP, Sicard GA. High-attenuating crescent in abdominal aortic aneurysm wall at CT: a sign of acute or impending rupture. Radiology 1994;192:359-62.
22. Simão da Silva E, Rodrigues AJ, Magalhãcs Castro de Tolosa E, Rodrigues CJ, Villas Boas do Prado G, Nakamoto JC. Morphology and diameter of infrarenal aortic aneurysms: a prospective autopsy study. Cardiovasc Surg 2000;8:526-32.
23. Swedenborg J, Labruto F, Roy J. Bleeding into the thrombus in ruptured abdominal aortic aneurysms. In: Greenhalgh RM, editor. More vascular and endovascular challenges. London: BIBA Publishing; 2007. p. 63-7.
24. Adolph R, Vorp DA, Steed DL, Webster MW, Kameneva MV, Watkins SC. Cellular content and permeability of intraluminal thrombus in abdominal aortic aneurysm. J Vasc Surg 1997;25:916-26.
25. Wang DH, Makaroun MS, Webster MW, Vorp DA. Mechanical properties and microstructure of intraluminal thrombus from abdominal aortic aneurysm. J Biomech Eng 2001;123:536-9.
26. Vande Geest JP, Sacks MS, Vorp DA. A planar biaxial constitutive relation for the luminal layer of intraluminal thrombus in abdominal aortic aneurysms. J Biomech 2006;39:2347-54.
27. van Dam EA, Dams SD, Peters GWM, Rutten MCM, Schurink GWH, Buth J, et al. Nonlinear viscoelastic behavior of abdominal aortic aneurysm thrombus. Biomech Model Mechanobio (Online 2007).
28. Ogden RW. Nonlinear elastic deformations. New York: Dover; 1997.
29. Fung YC. Biomechanics: mechanical properties of living tissue. New York: Springer-Verlag; 1981.
30. Fletcher R. Practical methods of optimization. New Delhi: John Wiley & Sons; 1989.
31. Zienkiewicz OC, Taylor RL. The finite element method. The basis, volume 1. 5th ed. Oxford: Butterworth Heinemann; 2000.
32. Holzapfel GA. Nonlinear solid mechanics. A continuum approach for engineering. Chichester: John Wiley & Sons; 2000.
33. Fung YC. Biomechanics. Mechanical properties of living tissues. 2nd ed New York: Springer-Verlag; 1993.
34. Suresh S. Fatigue of materials. 2nd ed. Cambridge, UK: Cambridge University Press; 1998.
35. Richardson PD. Biomechanics of plaque rupture: progress, problems, and new frontiers. Ann Biomed Eng 2002;30:524-36.
36. Sommer G, Gasser TC, Regitnig P, Auer M, Holzapfel GA. Dissection of the human aortic media: an experimental study. 2006 (in press).
37. Gasser TC, Holzapfel GA. Modeling dissection failure during balloon angioplasty. Ann Biomed Eng 2007;35:711-23.
38. Cowin SC, Bone mechanics handbook. Boca Raton, (FL): CRC Press, 2001.

Submitted Sep 28, 2007; accepted Jan 12, 2008.